A Digital Synthesis Model of Double-Reed Wind Instruments

Philippe Guillemain

A Digital Synthesis Model of Double-Reed Wind Instruments

Ph. Guillemain

Laboratoire de Mécanique et d'Acoustique, Centre National de la Recherche Scientifique, 31 chemin Joseph-Aiguier, 13402 Marseille cedex 20, France
Email: guillem@lma.cnrs-mrs.fr

We present a real-time synthesis model for double-reed wind instruments based on a nonlinear physical model. One specificity of double-reed instruments, namely, the presence of a confined air jet in the embouchure, for which a physical model has been proposed recently, is included in the synthesis model. The synthesis procedure involves the use of the physical variables via a digital scheme giving the impedance relationship between pressure and flow in the time domain. Comparisons are made between the behavior of the model with and without the confined air jet in the case of a simple cylindrical bore and that of a more realistic bore, the geometry of which is an approximation of an oboe bore.

Keywords and phrases: double-reed, synthesis, impedance.

1. INTRODUCTION

The simulation of woodwind instrument sounds has been investigated for many years since the pioneer studies by Schumacher [1] on the clarinet, which did not focus on digital sound synthesis. Real-time-oriented techniques, such as the famous digital waveguide method (see, e.g., Smith [2] and Välimäki [3]) and wave digital models [4] have been introduced in order to obtain efficient digital descriptions of resonators in terms of incoming and outgoing waves, and used to simulate various wind instruments.

The resonator of a clarinet can be said to be approximately cylindrical as a first approximation, and its embouchure is large enough to be compatible with simple airflow models. In double-reed instruments, such as the oboe, the resonator is not cylindrical but conical and the size of the air jet is comparable to that of the embouchure. In this case, the dissipation of the air jet is no longer free, and the jet remains confined in the embouchure, giving rise to additional aerodynamic losses.

Here, we describe a real-time digital synthesis model for double-reed instruments based on one hand on a recent study by Vergez et al. [5], in which the formation of the confined air jet in the embouchure is taken into account, and on the other hand on an extension of the method presented in [6] for synthesizing the clarinet. This method avoids the need for the incoming and outgoing wave decompositions, since it deals only with the relationship between the impedance variables, which makes it easy to transpose the physical model to a synthesis model.

The physical model is first summarized in Section 2. In order to obtain the synthesis model, a suitable form of the flow model is then proposed, a dimensionless version is written and the similarities with single-reed models (see, e.g., [7]) are pointed out. The resonator model is obtained by associating several elementary impedances, and is described in terms of the acoustic pressure and flow.

Section 3 presents the digital synthesis model, which requires first discrete-time equivalents of the reed displacement and the impedance relations. The explicit scheme solving the nonlinear model, which is similar to that proposed in [6], is then briefly summarized.

In Section 4, the synthesis model is used to investigate the effects of the changes in the nonlinear characteristics induced by the confined air jet.

2. PHYSICAL MODEL

The main physical components of the nonlinear synthesis model are as follows.

(i) The linear oscillator modeling the first mode of reeds vibration.
(ii) The nonlinear characteristics relating the flow to the pressure and to the reed displacement at the mouthpiece.
(iii) The impedance equation linking pressure and flow.

Figure 1 shows a highly simplified embouchure model for an oboe and the corresponding physical variables described in Sections 2.1 and 2.2.

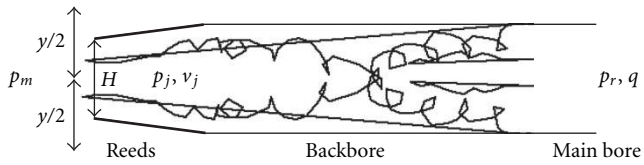

FIGURE 1: Embouchure model and physical variables.

2.1. Reed model

Although this paper focuses on the simulation of double-reed instruments, oboe experiments have shown that the displacements of the two reeds are symmetrical [5, 8]. In this case, a classical single-mode model seems to suffice to describe the variations in the reed opening. The opening is based on the relative displacement $y(t)$ of the two reeds when a difference in acoustic pressure occurs between the mouth pressure p_m and the acoustic pressure $p_j(t)$ of the air jet formed in the reed channel. If we denote the resonance frequency, damping coefficient, and mass of the reeds ω_r, q_r and μ_r, respectively, the relative displacement satisfies the equation

$$\frac{d^2y(t)}{dt^2} + \omega_r q_r \frac{dy(t)}{dt} + \omega_r^2 y(t) = -\frac{p_m - p_j(t)}{\mu_r}. \tag{1}$$

Based on the reed displacement, the opening of the reed channel denoted $S_i(t)$ is expressed by

$$S_i(t) = \Theta\big(y(t) + H\big) \times w\big(y(t) + H\big), \tag{2}$$

where w denotes the width of the reed channel, H denotes the distance between the two reeds at rest ($y(t)$ and $p_m = 0$) and Θ is the Heaviside function, the role of which is to keep the opening of the reeds positive by canceling it when $y(t) + H < 0$.

2.2. Nonlinear characteristics

2.2.1. Physical bases

In the case of the clarinet or saxophone, it is generally recognized that the acoustic pressure $p_r(t)$ and volume velocity $v_r(t)$ at the entrance of the resonator are equal to the pressure $p_j(t)$ and volume velocity $v_j(t)$ of the air jet in the reed channel (see, e.g., [9]). In oboe-like instruments, the smallness of the reed channel leads to the formation of a confined air jet. According to a recent hypothesis [5], $p_r(t)$ is no longer equal in this case to $p_j(t)$, but these quantities are related as follows

$$p_j(t) = p_r(t) + \frac{1}{2}\rho\Psi\frac{q(t)^2}{S_{ra}^2}, \tag{3}$$

where Ψ is taken to be a constant related to the ratio between the cross section of the jet and the cross section at the entrance of the resonator, $q(t)$ is the volume flow, and ρ is the mean air density. In what follows, we will assume that the area S_{ra}, corresponding to the cross section of the reed channel at the point where the flow is spread over the whole cross section, is equal to the area S_r at the entrance of the resonator.

The relationship between the mouth pressure p_m and the pressure of the air jet $p_j(t)$ and the velocity of the air jet $v_j(t)$ and the volume flow $q(t)$, classically used when dealing with single-reed instruments, is based on the stationary Bernoulli equation rather than on the Backus model (see, e.g., [10] for justification and comparisons with measurements). This relationship, which is still valid here, is

$$\begin{aligned} p_m &= p_j(t) + \frac{1}{2}\rho v_j(t)^2, \\ q(t) &= S_j(t)v_j(t) = \alpha S_i(t)v_j(t), \end{aligned} \tag{4}$$

where α, which is assumed to be constant, is the ratio between the cross section of the air jet $S_j(t)$ and the reed opening $S_i(t)$.

It should be mentioned that the aim of this paper is to propose a digital sound synthesis model that takes the dissipation of the air jet in the reed channel into account. For a detailed physical description of this phenomenon, readers can consult [5], from which the notation used here was borrowed.

2.2.2. Flow model

In the framework of the digital synthesis model on which this paper focuses, it is necessary to express the volume flow $q(t)$ as a function of the difference between the mouth pressure p_m and the pressure at the entrance of the resonator $p_r(t)$.

From (4), we obtain

$$v_j(t)^2 = \frac{2}{\rho}\big(p_m - p_j(t)\big), \tag{5}$$

$$q^2(t) = \alpha^2 S_i(t)^2 v_j(t)^2. \tag{6}$$

Substituting the value of $p_j(t)$ given by (3) into (5) gives

$$v_j(t)^2 = \frac{2}{\rho}\big(p_m - p_r(t)\big) - \Psi\frac{q(t)^2}{S_r^2}. \tag{7}$$

Using (6), this gives

$$q^2(t) = \alpha^2 S_i(t)^2\left(\frac{2}{\rho}\big(p_m - p_r(t)\big) - \Psi\frac{q(t)^2}{S_r^2}\right), \tag{8}$$

from which we obtain the expression for the volume flow, namely, the nonlinear characteristics

$$\begin{aligned} q(t) = {} & \operatorname{sign}\big(p_m - p_r(t)\big) \\ & \times \frac{\alpha S_i(t)}{\sqrt{1 + \Psi\alpha^2 S_i(t)^2/S_r^2}}\sqrt{\frac{2}{\rho}\,\big|\,p_m - p_r(t)\,\big|}. \end{aligned} \tag{9}$$

2.3. Dimensionless model

The reed displacement and the nonlinear characteristics are converted into the dimensionless equations used in the synthesis model. For this purpose, we first take the reed displacement equation and replace the air jet pressure $p_j(t)$ by the

expression involving the variables $q(t)$ and $p_r(t)$ (equation (3)),

$$\frac{d^2y(t)}{dt^2} + \omega_r q_r \frac{dy(t)}{dt} + \omega_r^2 y(t) = -\frac{p_m - p_r(t)}{\mu_r} + \rho\Psi\frac{q(t)^2}{2\mu_r S_r^2}. \tag{10}$$

On similar lines to what has been done in the case of single-reed instruments [11], $y(t)$ is normalized with respect to the static beating-reed pressure p_M defined by $p_M = H\omega_r^2\mu_r$. We denote by γ the ratio, $\gamma = p_m/p_M$ and replace $y(t)$ by $x(t)$, where the dimensionless reed displacement is defined by $x(t) = y(t)/H + \gamma$.

With these notations, (10) becomes

$$\frac{1}{\omega_r^2}\frac{d^2x(t)}{dt^2} + \frac{q_r}{\omega_r}\frac{dx(t)}{dt} + x(t) = \frac{p_r(t)}{p_M} + \frac{\rho\Psi}{2p_M}\frac{q(t)^2}{S_r^2} \tag{11}$$

and the reed opening is expressed by

$$S_i(t) = \Theta(1 - \gamma + x(t)) \times wH(1 - \gamma + x(t)). \tag{12}$$

Likewise, we use the dimensionless acoustic pressure $p_e(t)$ and the dimensionless acoustic flow $u_e(t)$ defined by

$$p_e(t) = \frac{p_r(t)}{p_M}, \qquad u_e(t) = \frac{\rho c}{S_r}\frac{q(t)}{p_M}, \tag{13}$$

where c is the speed of the sound.

With these notations, the reed displacement and the nonlinear characteristics are finally rewritten as follows,

$$\frac{1}{\omega_r^2}\frac{d^2x(t)}{dt^2} + \frac{q_r}{\omega_r}\frac{dx(t)}{dt} + x(t) = p_e(t) + \Psi\beta_u u_e(t)^2 \tag{14}$$

and using (9) and (12),

$$\begin{aligned} u_e(t) &= \Theta(1 - \gamma + x(t))\,\mathrm{sign}\,(\gamma - p_e(t)) \\ &\quad \times \frac{\zeta(1 - \gamma + x(t))}{\sqrt{1 + \Psi\beta_x(1 - \gamma + x(t))^2}}\sqrt{|\gamma - p_e(t)|} \\ &= \mathcal{F}(x(t), p_e(t)), \end{aligned} \tag{15}$$

where ζ, β_x and β_u are defined by

$$\zeta = \sqrt{H}\sqrt{\frac{2\rho}{\mu_r}}\frac{c\alpha w}{S_r\omega_r}, \qquad \beta_x = H^2\frac{\alpha^2 w^2}{S_r^2}, \qquad \beta_u = H\frac{\omega_r^2\mu_r}{2\rho c^2}. \tag{16}$$

This dimensionless model is comparable to the model described, for example, in [7, 9] in the case of single-reed instruments, where the dimensionless acoustic pressure $p_e(t)$, the dimensionless acoustic flow $u_e(t)$, and the dimensionless reed displacement $x(t)$ are linked by the relations

$$\begin{aligned} &\frac{1}{\omega_r^2}\frac{d^2x(t)}{dt^2} + \frac{q_r}{\omega_r}\frac{dx(t)}{dt} + x(t) = p_e(t), \\ &u_e(t) = \Theta(1 - \gamma + x(t))\,\mathrm{sign}\,(\gamma - p_e(t)) \\ &\qquad \times\zeta(1 - \gamma + x(t))\sqrt{|\gamma - p_e(t)|}. \end{aligned} \tag{17}$$

In addition to the parameter ζ, two other parameters β_x and β_u depend on the height H of the reed channel at rest. Although, for the sake of clarity in the notations, the variable t has been omitted, γ, ζ, β_x, and β_u are functions of time (but slowly varying functions compared to the other variables). Taking the difference between the jet pressure and the resonator pressure into account results in a flow which is no longer proportional to the reed displacement, and a reed displacement which is no longer linked to $p_e(t)$ in an ordinary linear differential equation.

2.4. Resonator model

We now consider the simplified resonator of an oboe-like instrument. It is described as a truncated, divergent, linear conical bore connected to a mouthpiece including the backbore to which the reeds are attached, and an additional bore, the volume of which corresponds to the volume of the missing part of the cone. This model is identical to that summarized in [12].

2.4.1. Cylindrical bore

The dimensionless input impedance of a cylindrical bore is first expressed. By assuming that the radius of the bore is large in comparison with the boundary layers thicknesses, the classical Kirchhoff theory leads to the value of the complex wavenumber for a plane wave $k(\omega) = \omega/c - (i^{3/2}/2)\eta c\omega^{1/2}$, where η is a constant depending on the radius R of the bore $\eta = (2/Rc^{3/2})(\sqrt{l_v} + (c_p/c_v - 1)\sqrt{l_t})$. Typical values of the physical constants, in mKs units, are $l_v = 4.10^{-8}$, $l_t = 5.6.10^{-8}$, $C_p/C_v = 1.4$ (see, e.g., [13]). The transfer function of a cylindrical bore of infinite length between $x = 0$ and $x = L$, which constitutes the propagation filter associated with the Green formulation, including the propagation delay, dispersion, and dissipation, is then given by $F(\omega) = \exp(-ik(\omega)L)$.

Assuming that the radiation losses are negligible, the dimensionless input impedance of the cylindrical bore is classically expressed by

$$\mathcal{C}(\omega) = i\tan(k(\omega)L). \tag{18}$$

In this equation, $\mathcal{C}(\omega)$ is the ratio between the Fourier transforms $P_e(\omega)$ and $U_e(\omega)$ of the dimensionless variables $p_e(t)$ and $u_e(t)$ defined by (13). The input admittance of the cylindrical bore is denoted by $\mathcal{C}^{-1}(\omega)$.

A different formulation of the impedance relation of a cylindrical bore, which is compatible with a time-domain implementation, and was proposed in [6], is used and extended here. It consists in rewriting (18) as

$$\mathcal{C}(\omega) = \frac{1}{1 + \exp(-2ik(\omega)L)} - \frac{\exp(-2ik(\omega)L)}{1 + \exp(-2ik(\omega)L)}. \tag{19}$$

Figure 2 shows the interpretation of (19) in terms of looped propagation filters. The transfer function of this model corresponds directly to the dimensionless input impedance of a cylindrical bore. It is the sum of two parts. The upper part corresponds to the first term of (19) and the

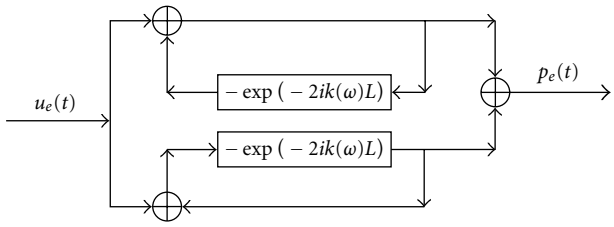

Figure 2: Impedance model of a cylindrical bore.

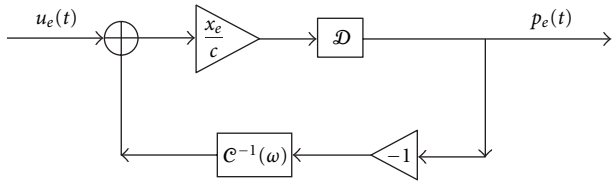

Figure 3: Impedance model of a conical bore.

lower part corresponds to the second term. The filter having the transfer function $-F(\omega)^2 = -\exp(-2ik(\omega)L)$ stands for the back and forth path of the dimensionless pressure waves, with a sign change at the open end of the bore.

Although $k(\omega)$ includes both dissipation and dispersion, the dispersion is small (e.g., in the case of a cylindrical bore with a radius of 7 mm, $\eta = 1.34.10^{-5}$), and the peaks of the input impedance of a cylindrical bore can be said to be nearly harmonic. In particular, this intrinsic dispersion can be neglected, unlike the dispersion introduced by the geometry of the bore (e.g., the input impedance of a truncated conical bore cannot be assumed to be harmonic).

2.4.2. Conical bore

From the input impedance of the cylindrical bore, the dimensionless input impedance of the truncated, divergent, conical bore can be expressed as a parallel combination of a cylindrical bore and an "air" bore,

$$\mathcal{Z}_2(\omega) = \frac{1}{1/(i\omega x_e/c) + 1/\mathcal{C}(\omega)}, \tag{20}$$

where x_e is the distance between the apex and the input. It is expressed in terms of the angle θ of the cone and the input radius R as $x_e = R/\sin(\theta/2)$.

The parameter η involved in the definition of $\mathcal{C}(\omega)$ in (20), which depends on the radius and characterizes the losses included in $k(\omega)$, is calculated by considering the radius of the cone at $(5/12)L$. This value was determined empirically, by comparing the impedance given by (20) with an input impedance of the same conical bore obtained with a series of elementary cylinders with different diameters (stepped cone), using the transmission line theory.

Denoting by $\mathcal{D}$ the differentiation operator $\mathcal{D}(\omega) = i\omega$ and rewriting (20) in the form $\mathcal{Z}_2(\omega) = \mathcal{D}(\omega)(x_e/c)/(1 + \mathcal{D}(\omega)(x_e/c)\mathcal{C}^{-1}(\omega))$, we propose the equivalent scheme in Figure 3.

2.4.3. Oboe-like bore

The complete bore is a conical bore combined with a mouthpiece.

The mouthpiece consists of a combination of two bores,

(i) a short cylindrical bore with length L_1, radius R_1, surface S_1, and characteristic impedance Z_1. This is the backbore to which the reeds are attached. Its radius is small in comparison with that of the main conical bore, the characteristic impedance of which is denoted $Z_2 = \rho c/S_r$, and

(ii) an additional short cylindrical bore with length L_0, radius R_0, surface S_0, and characteristic impedance Z_0. Its radius is large in comparison with that of the backbore. This role serves to add a volume corresponding to the truncated part of the complete cone. This makes it possible to reduce the geometrical dispersion responsible for inharmonic impedance peaks in the combination backbore/conical bore.

The impedance $\mathcal{C}_1(\omega)$ of the short cylindrical backbore is based on an approximation of $i\tan(k_1(\omega)L_1)$ with small values of $k_1(\omega)L_1$. It takes the dissipation into account and neglects the dispersion. Assuming that the radius R_1 is large in comparison with the boundary layers thicknesses, using (19), $\mathcal{C}_1(\omega)$ is first approximated by

$$\mathcal{C}_1(\omega) \simeq \frac{1 - \exp(-\eta_1 c\sqrt{\omega/2}L_1)\exp(-2i\omega L_1/c)}{1 + \exp(-\eta_1 c\sqrt{\omega/2}L_1)\exp(-2i\omega L_1/c)}, \tag{21}$$

which, since L_1 is small, is finally simplified as

$$\mathcal{C}_1(\omega) \simeq \frac{1 - \exp(-\eta_1 c\sqrt{\omega/2}L_1)(1 - 2i\omega L_1/c)}{1 + \exp(-\eta_1 c\sqrt{\omega/2}L_1)}. \tag{22}$$

By noting $G(\omega) = (1 - \exp(-\eta_1 c\sqrt{\omega/2}L_1))/(1 + \exp(-\eta_1 c\sqrt{\omega/2}L_1))$, and $H(\omega) = (L_1/c)(1 - G(\omega))$, the expression of $\mathcal{C}_1(\omega)$ reads

$$\mathcal{C}_1(\omega) = G(\omega) + i\omega H(\omega). \tag{23}$$

This approximation avoids the need for a second delay line in the sampled formulation of the impedance.

The transmission line equation relates the acoustic pressure p_n and the flow u_n at the entrance of a cylindrical bore (with characteristic impedance Z_n, length L_n, and wavenumber k_n) to the acoustic pressure p_{n+1} and the flow u_{n+1} at the exit of a cylindrical bore. With dimensioned variables, it reads

$$\begin{aligned} p_n(\omega) &= \cos(k_n(\omega)L_n)\,p_{n+1}(\omega) + iZ_n\sin(k_n(\omega)L_n)\,u_{n+1}(\omega), \\ u_n(\omega) &= \frac{i}{Z_n}\sin(k_n(\omega)L_n)\,p_{n+1}(\omega) + \cos(k_n(\omega)L_n)\,u_{n+1}(\omega), \end{aligned} \tag{24}$$

yielding

$$\frac{p_n(\omega)}{u_n(\omega)} = \frac{p_{n+1}(\omega)/u_{n+1}(\omega) + iZ_n\tan(k_n(\omega)L_n)}{1 + (i/Z_n)\tan(k_n(\omega)L_n)\,(p_{n+1}(\omega)/u_{n+1}(\omega))}. \tag{25}$$

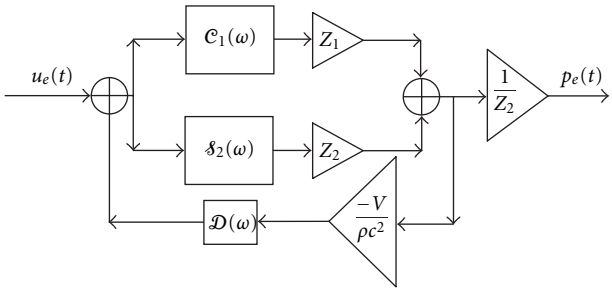

Figure 4: Impedance model of the simplified resonator.

Using the notations introduced in (20) and (23), the input impedance of the combination backbore/main conical bore reads

$$\frac{p_1(\omega)}{u_1(\omega)} = \frac{Z_2\mathcal{S}_2(\omega) + Z_1\mathcal{C}_1(\omega)}{1 + (Z_2/Z_1)\mathcal{S}_2(\omega)\mathcal{C}_1(\omega)}, \tag{26}$$

which is simplified as $p_1(\omega)/u_1(\omega) = Z_2\mathcal{S}_2(\omega) + Z_1\mathcal{C}_1(\omega)$, since $Z_1 \gg Z_2$.

In the same way, the input impedance of the whole bore reads

$$\frac{p_0(\omega)}{u_0(\omega)} = \frac{p_1(\omega)/u_1(\omega) + iZ_0\tan\left(k_0(\omega)L_0\right)}{1 + (i/Z_0)\tan\left(k_0(\omega)L_0\right)\left(p_1(\omega)/u_1(\omega)\right)}, \tag{27}$$

which, since $Z_0 \ll Z_1$, is simplified as

$$\frac{p_0(\omega)}{u_0(\omega)} = \frac{p_1(\omega)/u_1(\omega)}{1 + (i/Z_0)\tan\left(k_0(\omega)L_0\right)\left(p_1(\omega)/u_1(\omega)\right)}. \tag{28}$$

Since L_0 is small and the radius is large, the losses included in $k_0(\omega)$ can be neglected, and hence $k_0(\omega) = \omega/c$ and $\tan(k_0(\omega)L_0) = (\omega/c)L_0$. Under these conditions, the input impedance of the bore is given by

$$\begin{aligned}\frac{p_0(\omega)}{u_0(\omega)} &= \frac{1}{1/\left(p_1(\omega)/u_1(\omega)\right) + i\omega/c\left(L_0/Z_0\right)} \\ &= \frac{1}{1/\left(Z_2\mathcal{S}_2(\omega) + Z_1\mathcal{C}_1(\omega)\right) + i\omega/c\left(L_0S_0/\rho c\right)}.\end{aligned} \tag{29}$$

If we take V to denote the volume of the short additional bore $V = L_0S_0$ and rewrite (29) with the dimensionless variables P_e and U_e ($U_e = Z_2u_0$), the dimensionless input impedance of the whole resonator relating the variables $P_e(\omega)$ and $U_e(\omega)$ becomes

$$\begin{aligned}Z_e(\omega) &= \frac{P_e(\omega)}{U_e(\omega)} \\ &= \frac{1/Z_2}{i\omega V/\left(\rho c^2\right) + 1/\left(Z_1\mathcal{C}_1(\omega) + Z_2\mathcal{S}_2(\omega)\right)}.\end{aligned} \tag{30}$$

After rearranging (30), we propose the equivalent scheme in Figure 4.

It can be seen from (30) that the mouthpiece is equivalent to a Helmholtz resonator consisting of a hemispherical cavity with volume V and radius R_b such that $V = (4/6)\pi R_b^3$, connected to a short cylindrical bore with length L_1 and radius R_1.

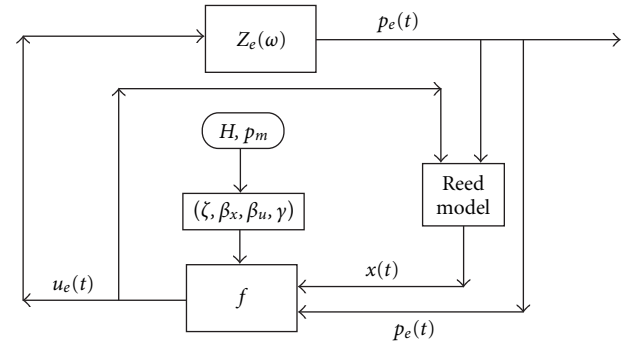

Figure 5: Nonlinear synthesis model.

2.5. Summary of the physical model

The complete dimensionless physical model consists of three equations,

$$\frac{1}{\omega_r^2}\frac{d^2x(t)}{dt^2} + \frac{q_r}{\omega_r}\frac{dx(t)}{dt} + x(t) = p_e(t) + \Psi\beta_u u_e(t)^2, \tag{31}$$

$$\begin{aligned}u_e(t) = {} & \frac{\zeta\left(1 - \gamma + x(t)\right)}{\sqrt{1 + \Psi\beta_x\left(1 - \gamma + x(t)\right)^2}} \\ & \times \Theta\left(1 - \gamma + x(t)\right)\operatorname{sign}\left(\gamma - p_e(t)\right) \times \sqrt{\left|\gamma - p_e(t)\right|},\end{aligned} \tag{32}$$

$$P_e(\omega) = Z_e(\omega)U_e(\omega). \tag{33}$$

These equations enable us to introduce the reed and the nonlinear characteristics in the form of two nonlinear loops, as shown in Figure 5. The first loop relates the output p_e to the input u_e of the resonator, as in the case of single-reed instruments models. The second nonlinear loop corresponds to the u_e^2-dependent changes in x. The output of the model is given by the three coupled variables p_e, u_e, and x. The control parameters of the model are the length L of the main conical bore and the parameters $H(t)$ and $p_m(t)$ from which $\zeta(t)$, $\beta_x(t)$, $\beta_u(t)$, and $\gamma(t)$ are calculated.

In the context of sound synthesis, it is necessary to calculate the external pressure. Here we consider only the propagation within the main "cylindrical" part of the bore in (20). Assuming again that the radiation impedance can be neglected, the external pressure corresponds to the time derivative of the flow at the exit of the resonator $p_{\text{ext}}(t) = du_s(t)/dt$. Using the transmission line theory, one directly obtains

$$U_s(\omega) = \exp\left(-ik(\omega)L\right)\left(P_e(\omega) + U_e(\omega)\right). \tag{34}$$

From the perceptual point of view, the quantity $\exp(-ik(\omega)L)$ can be left aside, since it stands for the losses corresponding to a single travel between the embouchure and the open end. This simplification leads to the following expression for the external pressure

$$p_{\text{ext}}(t) = \frac{d}{dt}\left(p_e(t) + u_e(t)\right). \tag{35}$$

3. DISCRETE-TIME MODEL

In order to draw up the synthesis model, it is necessary to use a discrete formulation in the time domain for the reed displacement and the impedance models. The discretization schemes used here are similar to those described in [6] for the clarinet, and summarized in [12] for brass instruments and saxophones.

3.1. Reed displacement

We take $e(t)$ to denote the excitation of the reed $e(t) = p_e(t) + \Psi\beta_u u_e(t)^2$. Using (31), the Fourier transform of the ratio $X(\omega)/E(\omega)$ can be readily written as

$$\frac{X(\omega)}{E(\omega)} = \frac{\omega_r^2}{\omega_r^2 - \omega^2 + i\omega q_r \omega_r}. \tag{36}$$

An inverse Fourier transform provides the impulse response $h(t)$ of the reed model

$$h(t) = \frac{2\omega_r}{\sqrt{4 - q_r^2}} \exp\left(-\frac{1}{2}\omega_r q_r t\right) \sin\left(\frac{1}{2}\sqrt{4 - q_r^2}\,\omega_r t\right). \tag{37}$$

Equation (37) shows that $h(t)$ satisfies $h(0) = 0$. This property is most important in what follows. In addition, the range of variations allowed for q_r is $]0, 2[$.

The discrete-time version of the impulse response uses two centered numerical differentiation schemes which provide unbiased estimates of the first and second derivatives when they are applied to sampled second-order polynomials

$$\begin{aligned} i\omega &\simeq \frac{f_e}{2}(z - z^{-1}), \\ -\omega^2 &\simeq f_e^2(z - 2 + z^{-1}), \end{aligned} \tag{38}$$

where $z = \exp(i\tilde{\omega})$, $\tilde{\omega} = \omega/f_e$, and f_e is the sampling frequency.

With these approximations, the digital transfer function of the reed is given by

$$\frac{X(z)}{E(z)} = \frac{z^{-1}}{f_e^2/\omega_r^2 + f_e q_r/(2\omega_r) - z^{-1}(2f_e^2/\omega_r^2 - 1) - z^{-2}(f_e q_r/(2\omega_r) - f_e^2/\omega_r^2)}, \tag{39}$$

yielding a difference equation of the type

$$x(n) = b_{1_a} e(n-1) + a_{1_a} x(n-1) + a_{2_a} x(n-2). \tag{40}$$

This difference equation keeps the property $h(0) = 0$.

Figure 6 shows the frequency response of this approximated reed model (solid line) superimposed with the exact one (dotted line).

This discrete reed model is stable under the condition $\omega_r < f_e\sqrt{4 - q_r^2}$. Under this condition, the modulus of the poles of the transfer function is given by $\sqrt{(2f_e - \omega_r q_r)/(2f_e + \omega_r q_r)}$ and is always smaller than 1. This stability condition makes this discretization scheme unsuitable for use at low sampling rates, but in practice, at the CD quality sample rate, this problem does not arise for a reed resonance frequency of up to 5 kHz with a quality factor of up to 0.5. For a more detailed discussion of discretization schemes, readers can consult, for example, [14].

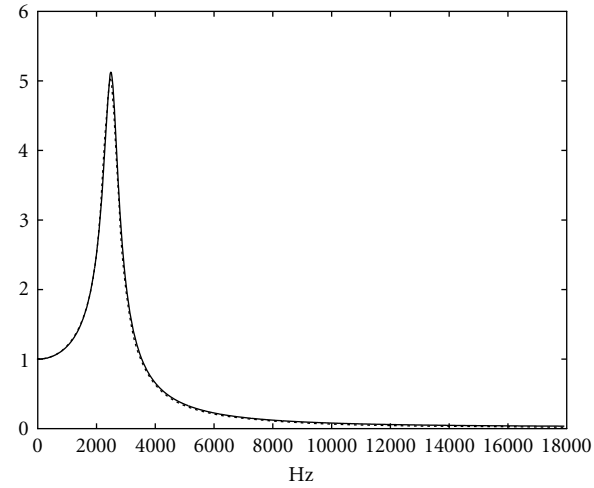

FIGURE 6: Approximated (solid line) and exact (dotted line) reed frequency response with parameter values $f_r = 2500$ Hz, $q_r = 0.2$, and $f_e = 44.1$ kHz.

The bilinear transformation does not provide a suitable discretization scheme for the reed displacement. In this case, the impulse response does not satisfy the property of the continuous model $h(0) = 0$.

3.2. Impedance

A time domain equivalent to the inverse Fourier transform of impedance $Z_e(\omega)$ given by (30) is now required. Here we express $p_e(n)$ as a function of $u_e(n)$.

The losses in the cylindrical bore element contributing to the impedance of the whole bore are modeled with a digital low-pass filter. This filter approximates the back and forth losses described by $F(\omega)^2 = \exp(-2ik(\omega)L)$ and neglects the (small) dispersion. So that they can be adjusted to the geometry of the resonator, the coefficients of the filter are expressed analytically as functions of the physical parameters, rather than using numerical approximations and minimizations. For this purpose, a one-pole filter is used,

$$\tilde{F}(\tilde{\omega}) = \frac{b_0 \exp(-i\tilde{\omega}D)}{1 - a_1 \exp(-i\tilde{\omega})}, \tag{41}$$

where $\tilde{\omega} = \omega/f_e$, and $D = 2f_e(L/c)$ is the pure delay corresponding to a back and forth path of the waves.

The parameters b_0 and a_1 are calculated so that $|F(\omega)^2|^2 = |\tilde{F}(\tilde{\omega})|^2$ for two given values of ω, and are solutions of the system

$$\begin{aligned} \left|F(\omega_1)^2\right|^2 (1 + a_1^2 - 2a_1\cos(\tilde{\omega}_1)) &= b_0^2, \\ \left|F(\omega_2)^2\right|^2 (1 + a_1^2 - 2a_1\cos(\tilde{\omega}_2)) &= b_0^2, \end{aligned} \tag{42}$$

where $|F(\omega_{(1,2)})^2|^2 = \exp(-2\eta c\sqrt{\omega_{(1,2)}/2}L)$. The first value ω_1 is an approximation of the frequency of the first impedance peak of the truncated conical bore given by $\omega_1 = c(12\pi L+9\pi^2 x_e+16L)/(4L(4L+3\pi x_e+4x_e))$, in order to ensure a suitable height of the impedance peak at the fundamental frequency. It is important to keep this feature to obtain a realistic digital simulation of the continuous dynamical system, since the linear impedance is associated with the nonlinear characteristics. This ensures that the decay time of the fundamental frequency of the approximated impulse response of the impedance matches the exact value, which is important in the case of fast changes in γ (e.g., attack transient). The second value ω_2 corresponds to the resonance frequency of the Helmholz resonator $\omega_2 = c\sqrt{S_1/(L_1 V)}$.

The phase of $\tilde{F}(\tilde{\omega})$ has a nonlinear part, which is given by $-\arctan(a_1 \sin(\tilde{\omega})/(1 - a_1 \cos(\tilde{\omega})))$. This part differs from the nonlinear part of the phase of $F(\omega)^2$, which is given by $-\eta c\sqrt{\omega/2}L$. Although these two quantities are different and although the phase of $\tilde{F}(\tilde{\omega})$ is determined by the choice of a_1, which is calculated from the modulus, it is worth noting that in both cases, the dispersion is always very small, has a negative value, and is monotonic up to the frequency $(f_e/2\pi)\arccos(a_1)$. Consequently, in both cases, in the case of a cylindrical bore, up to this frequency, the distance between successive impedance peaks decreases as their rank increases, $\omega_{n+1} - \omega_n < \omega_n - \omega_{n-1}$.

Using (19) and (41), the impedance of the cylindrical bore unit $\mathcal{C}(\omega)$ is then expressed by

$$\mathcal{C}(z) = \frac{1 - a_1 z^{-1} - b_0 z^{-D}}{1 - a_1 z^{-1} + b_0 z^{-D}}. \tag{43}$$

Since L_1 is small, the frequency-dependent function $G(\omega)$ involved in the definition of the impedance of the short backbore $\mathcal{C}_1(\omega)$ can be approximated by a constant, corresponding to its value in ω_2.

The bilinear transformation is used to discretize $\mathcal{D} = i\omega$: $D(z) = 2f_e((z-1)/(z+1))$.

The combination of all these parts according to (30) yields the digital impedance of the whole bore in the form

$$Z_e(z) = \frac{\sum_{k=0}^{k=4} b_{c_k} z^{-k} + \sum_{k=0}^{k=3} b_{c_{Dk}} z^{-D-k}}{1 - \sum_{k=1}^{k=4} a_{c_k} z^{-k} - \sum_{k=0}^{k=3} a_{c_{Dk}} z^{-D-k}}, \tag{44}$$

where the coefficients b_{c_k}, a_{c_k}, $b_{c_{Dk}}$, and $a_{c_{Dk}}$ are expressed analytically as functions of the geometry of each part of the bore. This leads directly to the difference equation, which can be conveniently written in the form

$$p_e(n) = b_{c_0} u_e(n) + \tilde{V}, \tag{45}$$

where $\tilde{V}$ includes all the terms that do not depend on the time sample n

$$\begin{aligned}\tilde{V} = &\sum_{k=1}^{k=4} b_{c_k} u_e(n-k) + \sum_{k=0}^{k=3} b_{c_{Dk}} u_e(n-D-k) \\ &+ \sum_{k=1}^{k=4} a_{c_k} p_e(n-k) + \sum_{k=0}^{k=3} a_{c_{Dk}} p_e(n-D-k).\end{aligned} \tag{46}$$

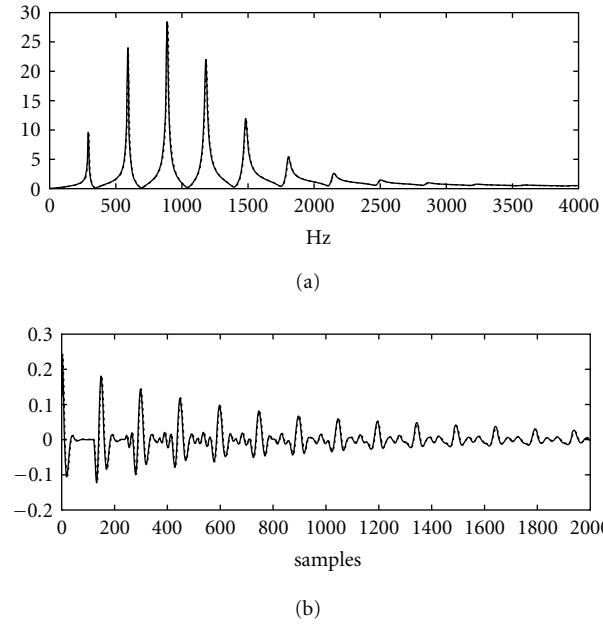

Figure 7: (a) represents approximated (solid lines) and exact (dotted lines) input impedance, while (b) represents approximated (solid lines) and exact (dotted lines) impulse response. Geometrical parameters $L = 0.46\,\text{m}$, $R = 0.00216\,\text{m}$, $\theta = 2^\circ$, $L_1 = 0.02\,\text{m}$, $R_1 = 0.0015\,\text{m}$, and $R_b = 0.006\,\text{m}$.

Figure 7 shows an oboe-like bore input impedance, both approximated (solid line) and exact (dotted line) together with the corresponding impulse responses.

3.3. Synthesis algorithm

The sampled expressions for the impulse responses of the reed displacement and the impedance models are now used to write the sampled equivalent of the system of (31), (32), and (33):

$$\begin{aligned}x(n) = {} & b_{1_a}(p_e(n-1) + \Psi\beta_u u_e(n-1)^2) \\ & + a_{1_a} x(n-1) + a_{2_a} x(n-2),\end{aligned} \tag{47}$$

$$p_e(n) = b_{c_0} u_e(n) + \tilde{V}, \tag{48}$$

$$u_e(n) = W \operatorname{sign}(\gamma - p_e(n))\sqrt{|\gamma - p_e(n)|}, \tag{49}$$

where W is

$$\begin{aligned}W = {} & \Theta(1 - \gamma + x(n)) \\ & \times \frac{\zeta(1 - \gamma + x(n))}{\sqrt{1 + \Psi\beta_x(1 - \gamma + x(n))^2}}.\end{aligned} \tag{50}$$

This system of equations is an implicit system, since $u_e(n)$ has to be known in order to be able to compute $p_e(n)$ with the impedance equation (48). Likewise, $u_e(n)$ is obtained from the nonlinear equation (49) and requires $p_e(n)$ to be known.

Thanks to the specific reed discretization scheme presented in Section 3.1, calculating $x(n)$ with (47) does not

require $p_e(n)$ and $u_e(n)$ to be known. This makes it possible to solve this system explicitly, as shown in [6], thus doing away with the need for schemes such as the **K**-method [15].

Since W is always positive, if one considers the two cases $\gamma - p_e(n) \geq 0$ and $\gamma - p_e(n) < 0$, successively, substituting the expression for $p_e(n)$ from (48) into (49) eventually gives

$$u_e(n) = \frac{1}{2}\,\mathrm{sign}(\gamma - \tilde{V}) \times \left(- b_{c_0} W^2 + W\sqrt{(b_{c_0} W)^2 + 4|\gamma - \tilde{V}|}\right). \tag{51}$$

The acoustic pressure and flow in the mouthpiece at sampling time n are then finally obtained by the sequential calculation of $\tilde{V}$ with (46), $x(n)$ with (47), W with (50), $u_e(n)$ with (51), and $p_e(n)$ with (48).

The external pressure $p_{\mathrm{ext}}(n)$ is calculated using the difference between the sum of the internal pressure and the flow at sampling time n and $n-1$.

4. SIMULATIONS

The effects of introducing the confined air jet into the nonlinear characteristics are now studied in the case of two different bore geometries. In particular, we consider a cylindrical resonator, the impedance peaks of which are odd harmonics, and a resonator, the impedance of which contains all the harmonics. We start by checking numerically the validity of the resolution scheme in the case of the cylindrical bore. (Sound examples are available at http://omicron.cnrs-mrs.fr/~guillemain/eurasip.html.)

4.1. Cylindrical resonator

We first consider a cylindrical resonator, and make the parameter Ψ vary linearly from 0 to 4000 during the sound synthesis procedure (1.5 seconds). The transient attack corresponds to an abrupt increase in γ at $t = 0$. During the decay phase, starting at $t = 1.3$ seconds, γ decreases linearly towards zero. Its steady-state value is $\gamma = 0.56$. The other parameters are constant, $\zeta = 0.35$, $\beta_x = 7.5.10^{-4}$, $\beta_u = 6.1.10^{-3}$. The reed parameters are $\omega_r = 2\pi.3150$ rad/second, $q_r = 0.5$. The resonator parameters are $R = 0.0055$ m, $L = 0.46$ m.

Figure 8 shows superimposed curves, in the top figure, the digital impedance of the bore is given in dotted lines, and the ratio between the Fourier transforms of the signals $p_e(n)$ and $u_e(n)$ in solid lines; in the bottom figure, the digital reed transfer function is given in dotted lines, and the ratio of the Fourier transforms of the signals $x(n)$ and $p_e(n)+\Psi(n)\beta_u u_e(n)^2$ (including attack and decay transients) in solid lines.

As we can see, the curves are perfectly superimposed. There is no need to check the nonlinear relation between $u_e(n)$, $p_e(n)$, and $x(n)$, which is satisfied by construction since $u_e(n)$ is obtained explicitly as a function of the other variables in (51). In the case of the oboe-like bore, the results obtained using the resolution scheme are equally accurate.

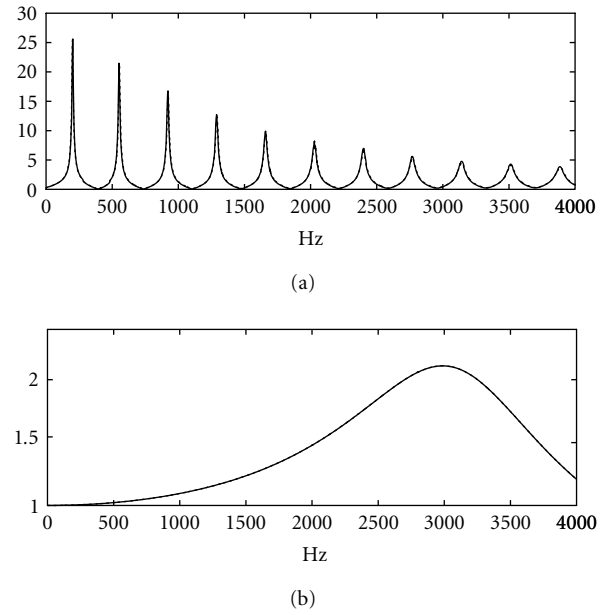

FIGURE 8: (a) represents impedance (dotted line) and ratio between the spectra of p_e and u_e (solid line), while (b) represents reed transfer (dotted line) and ratio of spectra between x and $p_e+\Psi\beta_u u_e^2$ (solid line).

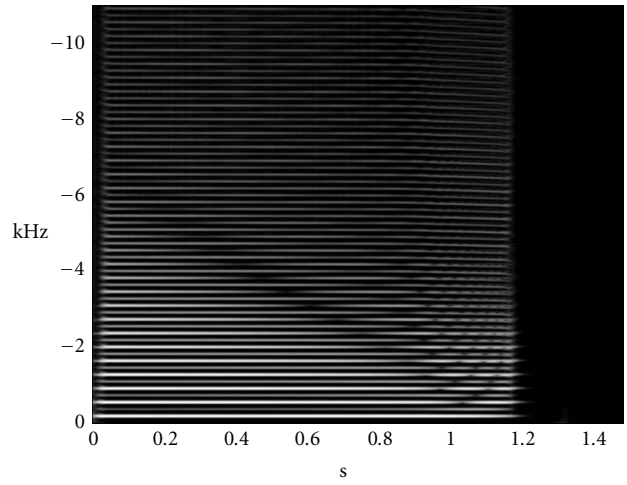

FIGURE 9: Spectrogram of the external pressure for a cylindrical bore and a beating reed where $\gamma = 0.56$.

4.1.1. The case of the beating reed

The first example corresponds to a beating reed situation, which is simulated by choosing a steady-state value of γ greater than 0.5 ($\gamma = 0.56$).

Figure 9 shows the spectrogram (dB) of the external pressure generated by the model. The values of the spectrogram are coded with a grey-scale palette (small values are dark and high values are bright). The bright horizontal lines correspond to the harmonics of the external pressure.

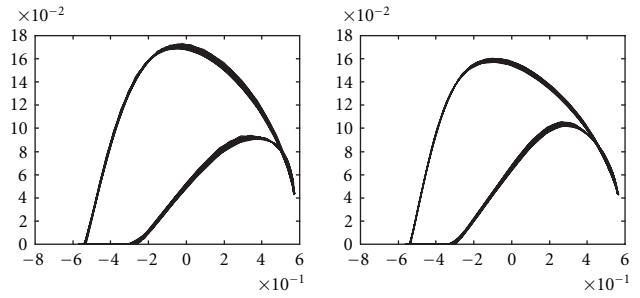

FIGURE 10: $u_e(n)$ versus $p_e(n)$: (a) $t = 0.25$ second, (b) $t = 0.5$ second.

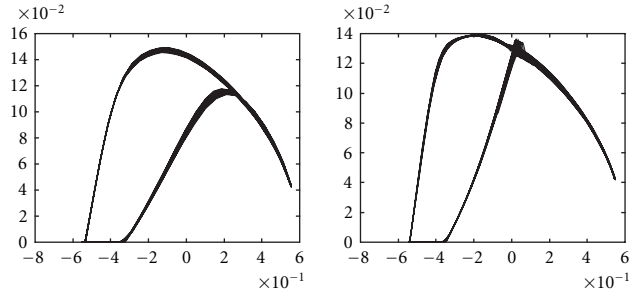

FIGURE 11: $u_e(n)$ versus $p_e(n)$: (a) $t = 0.75$ second, (b) $t = 1$ second.

Increasing the value of Ψ mainly affects the pitch and only slightly affects the amplitudes of the harmonics. In particular, at high values of Ψ, a small increase in Ψ results in a strong decrease in the pitch.

A cancellation of the self-oscillation process can be observed at around $t = 1.2$ seconds, due to the high value of Ψ, since it occurs before γ starts decreasing.

Odd harmonics have a much higher level than even harmonics as occuring in the case of the clarinet. Indeed, the even harmonics originate mainly from the flow, which is taken into account in the calculation of the external pressure. However, it is worth noticing that the level of the second harmonic increases with Ψ.

Figures 10 and 11 show the flow $u_e(n)$ versus the pressure $p_e(n)$, obtained during a small number (32) of oscillation periods at around $t = 0.25$ seconds, $t = 0.5$ seconds, $t = 0.75$ seconds and $t = 1$ seconds. The existence of two different paths, corresponding to the opening or closing of the reed, is due to the inertia of the reed. This phenomenon is observed also on single-reed instruments (see, e.g., [14]). A discontinuity appears in the whole path because the reed is beating. This cancels the opening (and hence the flow) while the pressure is still varying.

The shape of the curve changes with respect to Ψ. This shape is in agreement with the results presented in [5].

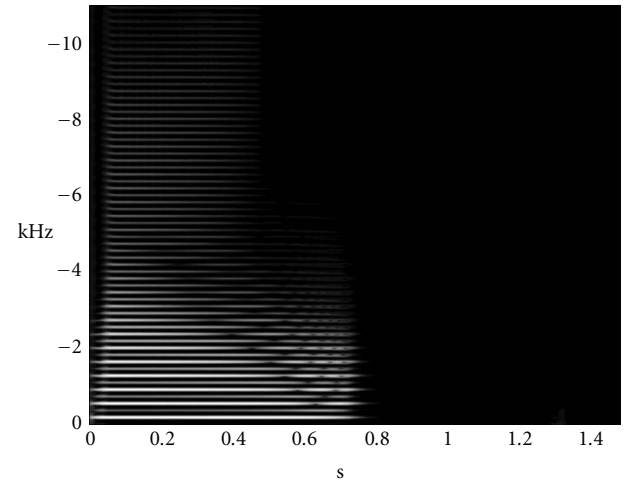

FIGURE 12: Spectrogram of the external pressure for a cylindrical bore and a nonbeating reed where $\gamma = 0.498$.

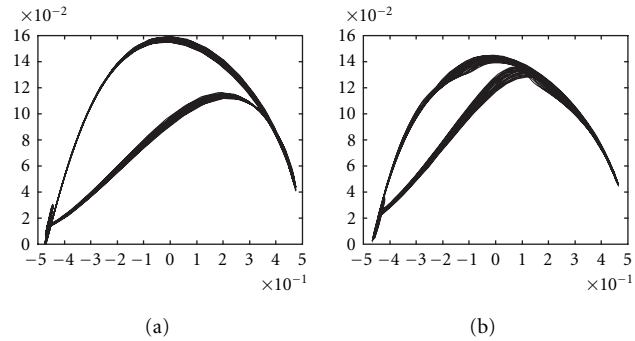

FIGURE 13: $u_e(n)$ versus $p_e(n)$: (a) $t = 0.25$ second, (b) $t = 0.5$ second.

4.1.2. The case of the nonbeating reed

The second example corresponds to a nonbeating reed situation, which is obtained by choosing a steady-state value of γ smaller than 0.5 ($\gamma = 0.498$).

Figure 12 shows the spectrogram of the external pressure generated by the model. Increasing the value of Ψ results in a sharp change in the level of the high harmonics at around $t = 0.4$ seconds, a slight change in the pitch, and a cancellation of the self-oscillation process at around $t = 0.8$ seconds, corresponding to a smaller value of Ψ than that observed in the case of the beating reed.

Figure 13 shows the flow $u_e(n)$ versus the pressure $p_e(n)$ at around $t = 0.25$ seconds and $t = 0.5$ seconds. Since the reed is no longer beating, the whole path remains continuous. The changes in its shape with respect to Ψ are smaller than in the case of the beating reed.

4.2. Oboe-like resonator

In order to compare the effects of the confined air jet with the geometry of the bore, we now consider an oboe-like bore,

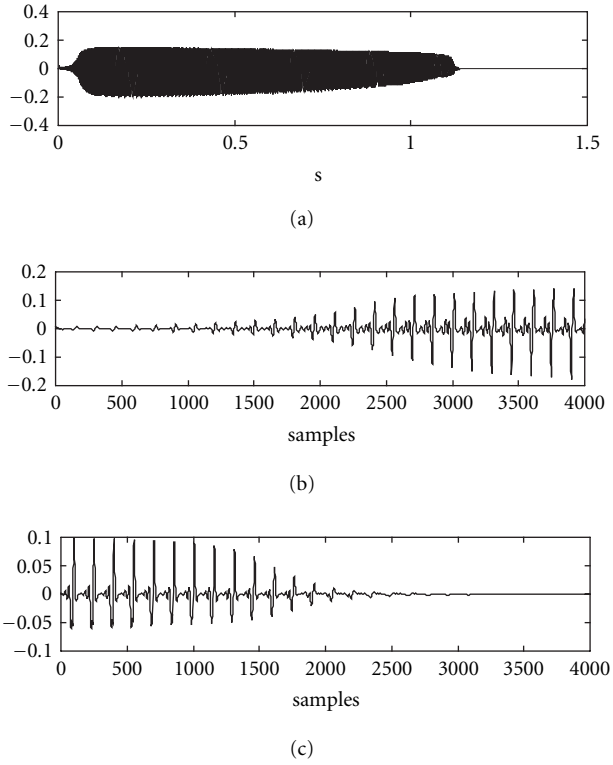

FIGURE 14: (a) represents external acoustic pressure, and (b), (c) represent attack and decay transients.

the input impedance, and geometric parameters of which correspond to Figure 7. The other parameters have the same values as in the case of the cylindrical resonator, and the steady-state value of γ is $\gamma = 0.4$.

Figure 14 shows the pressure $p_{\text{ext}}(t)$. Increasing the effect of the air jet confinement with Ψ, and hence the aerodynamical losses, results in a gradual decrease in the signal amplitude. The change in the shape of the waveform with respect to Ψ can be seen on the blowups corresponding to the attack and decay transients.

Figure 15 shows the spectrogram of the external pressure generated by the model.

Since the impedance includes all the harmonics (and not only the odd ones as in the case of the cylindrical bore), the output pressure also includes all the harmonics. This makes for a considerable perceptual change in the timbre in comparison with the cylindrical geometry. Since the input impedance of the bore is not perfectly harmonic, it is not possible to determine whether the "moving formants" are caused by a change in the value of Ψ or by a "phasing effect" resulting from the slight inharmonic nature of the impedance.

Increasing the value of Ψ affects the amplitude of the harmonics and slightly changes the pitch. In addition, as in the case of the cylindrical bore with a nonbeating reed, a large value of Ψ brings the self-oscillation process to an end.

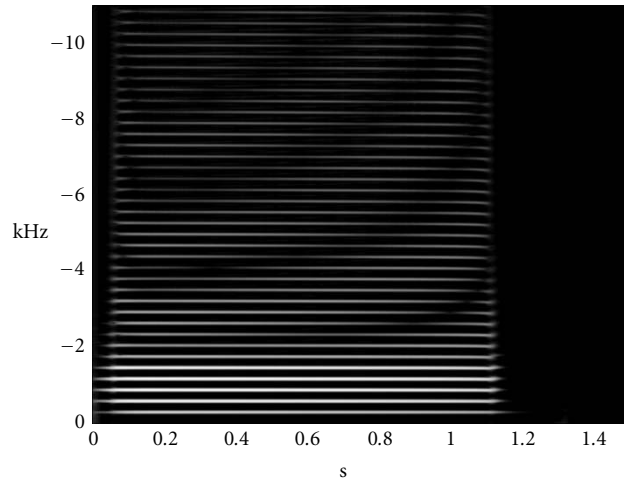

FIGURE 15: Spectrogram of the external pressure for an oboe-like bore where $\gamma = 0.4$.

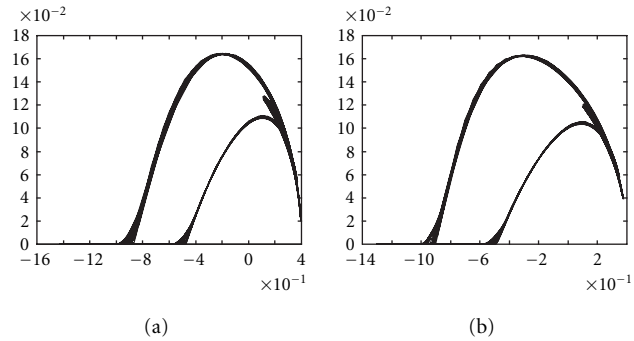

FIGURE 16: $u_e(n)$ versus $p_e(n)$: (a) $t = 0.25$ second, (b) $t = 0.5$ second.

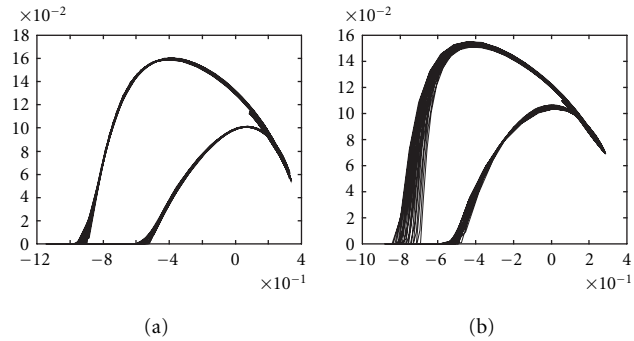

FIGURE 17: $u_e(n)$ versus $p_e(n)$: (a) $t = 0.75$ second, (b) $t = 1$ second.

Figures 16 and 17 show the flow $u_e(n)$ versus the pressure $p_e(n)$ at around $t = 0.25$ seconds, $t = 0.5$ seconds, $t = 0.75$ seconds, and $t = 1$ seconds. The shape and evolution with Ψ of the nonlinear characteristics are similar to what occurs in the case of a cylindrical bore with a beating reed.

5. CONCLUSION

The synthesis model described in this paper includes the formation of a confined air jet in the embouchure of double-reed instruments. A dimensionless physical model, the form of which is suitable for transposition to a digital synthesis model, is proposed. The resonator is modeled using a time domain equivalent of the input impedance and does not require the use of wave variables. This facilitates the modeling of the digital coupling between the bore, the reed and the nonlinear characteristics, since all the components of the model use the same physical variables. It is thus possible to obtain an explicit resolution of the nonlinear coupled system thanks to the specific discretization scheme of the reed model. This is applicable to other self-oscillating wind instruments using the same flow model, but it still requires to be compared with other methods.

This synthesis model was used in order to study the influence of the confined jet on the sound generated, by carrying out a real-time implementation. Based on the results of informal listening tests with an oboe player, the sound and dynamics of the transients obtained are fairly realistic. The simulations show that the shape of the resonator is the main factor determining the timbre of the instrument in steady-state parts, and that the confined jet plays a role at the control level of the model, since it increases the oscillation step and therefore plays an important role mainly in the transient parts.

ACKNOWLEDGMENTS

The author would like to thank Christophe Vergez for helpful discussions on the physical flow model, and Jessica Blanc for reading the English.

REFERENCES

[1] R. T. Schumacher, "Ab initio calculations of the oscillation of a clarinet," *Acustica*, vol. 48, no. 71, pp. 71–85, 1981.

[2] J. O. Smith III, "Principles of digital waveguide models of musical instruments," in *Applications of Digital Signal Processing to Audio and Acoustics*, M. Kahrs and K. Brandenburg, Eds., pp. 417–466, Kluwer Academic Publishers, Boston, Mass, USA, 1998.

[3] V. Välimäki and M. Karjalainen, "Digital waveguide modeling of wind instrument bores constructed of truncated cones," in *Proc. International Computer Music Conference*, pp. 423–430, Computer Music Association, San Francisco, 1994.

[4] M. van Walstijn and M. Campbell, "Discrete-time modeling of woodwind instrument bores using wave variables," *Journal of the Acoustical Society of America*, vol. 113, no. 1, pp. 575–585, 2003.

[5] C. Vergez, R. Almeida, A. Caussé, and X. Rodet, "Toward a simple physical model of double-reed musical instruments: influence of aero-dynamical losses in the embouchure on the coupling between the reed and the bore of the resonator," *Acustica*, vol. 89, pp. 964–974, 2003.

[6] Ph. Guillemain, J. Kergomard, and Th. Voinier, "Real-time synthesis of wind instruments, using nonlinear physical models," submitted to Journal of the Acoustical Society of America.

[7] J. Kergomard, "Elementary considerations on reed-instrument oscillations," in *Mechanics of Musical Instruments*, A. Hirschberg, J. Kergomard, and G. Weinreich, Eds., Springer-Verlag, New York, NY, USA, 1995.

[8] A. Almeida, C. Vergez, R. Caussé, and X. Rodet, "Physical study of double-reed instruments for application to sound-synthesis," in *Proc. International Symposium in Musical Acoustics*, pp. 221–226, Mexico City, Mexico, December 2002.

[9] A. Hirschberg, "Aero-acoustics of wind instruments," in *Mechanics of Musical Instruments*, A. Hirschberg, J. Kergomard, and G. Weinreich, Eds., Springer-Verlag, New York, NY, USA, 1995.

[10] S. Ollivier, *Contribution à l'étude des oscillations des instruments à vent à anche simple*, Ph.D. thesis, l'Université du Maine, France, 2002.

[11] T. A. Wilson and G. S. Beavers, "Operating modes of the clarinet," *Journal of the Acoustical Society of America*, vol. 56, no. 2, pp. 653–658, 1974.

[12] Ph. Guillemain, J. Kergomard, and Th. Voinier, "Real-time synthesis models of wind instruments based on physical models," in *Proc. Stockholm Music Acoustics Conference*, Stockholm, Sweden, 2003.

[13] A. D. Pierce, *Acoustics—An Introduction to Its Physical Principles and Applications*, McGraw-Hill, New York, NY, USA, 1981, reprinted by Acoustical Society of America, Woodbury, NY, USA, 1989.

[14] F. Avanzini and D. Rocchesso, "Efficiency, accuracy, and stability issues in discrete time simulations of single reed instruments," *Journal of the Acoustical Society of America*, vol. 111, no. 5, pp. 2293–2301, 2002.

[15] G. Borin, G. De Poli, and D. Rocchesso, "Elimination of delay-free loops in discrete-time models of nonlinear acoustic systems," *IEEE Trans. Speech and Audio Processing*, vol. 8, no. 5, pp. 597–605, 2000.